NAR Genomics and Bioinformatics, 2024, **6**, lqae155
https://doi.org/10.1093/nargab/lqae155
Advance access publication date: 28 November 2024
Standard Article

Comparative molecular dynamics calculations of duplexation of chemically modified analogs of DNA used for antisense applications

Rodrigo Galindo-Murillo[1], Jack S. Cohen[2] and Barak Akabayov[2,*]

[1]Department of Medicinal Chemistry, Ionis Pharmaceuticals, 2855 Gazelle Court, Carlsbad, CA 92010, USA
[2]Department of Chemistry, Ben Gurion University of the Negev, Beer Sheva, 8410501, Israel
[*]To whom correspondence should be addressed. Email: akabayov@bgu.ac.il

Abstract

We have subjected several analogs of DNA that have been widely used as antisense oligonucleotide (ASO) inhibitors of gene expression to comparative molecular dynamics (MD) calculations of their ability to form duplexes with DNA and RNA. The analogs included in this study are the phosphorothioate (PS), peptide nucleic acid (PNA), locked nucleic acid (LNA), morpholino nucleic acid (PMO), the 2′-OMe, 2′-F, 2′-methoxyethyl (2′-MOE) and the constrained cET analogs, as well as the natural phosphodiester (PO) as control, for a total of nine structures, in both XNA–DNA and XNA–RNA duplexes. This is intended as an objective criterion for their relative ability to duplex with an RNA complement and their comparative potential for antisense applications. We have found that the constrained furanose ring analogs show increased stability when considering this study's structural and energetic parameters. The 2′-MOE modification, even though energetically stable, has an elevated dynamic range and breathing properties due to the bulkier moiety in the C2′ position of the furanose. The smaller modifications in the C2′ position, 2′-F, 2′-OMe and PS also form stable and energetically favored duplexes with both DNA and RNA. The morpholino moiety allows for increased tolerance in accommodating either DNA or RNA and the PNA, with the PNA being the most energetically stable, although with a preference for the B-form DNA. In summary, we can rank the overall preference of hybrid strand formations as PNA > cET/LNA > PS/2′-F/2′-OMe > morpholino > 2′-MOE for the efficacy of duplex formation.

Graphical abstract

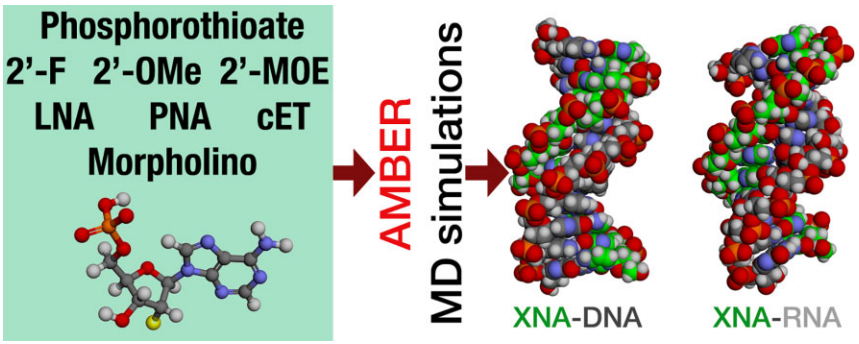

Introduction

The first reported use of an oligodeoxynucleotide for antisense inhibition was by Zamecnik and Stephenson against the Rous sarcoma virus in 1978 using a natural phosphodiester oligomer (1). However, people had difficulty reproducing this result, probably due to the prevalence of natural nucleases *in vitro* (2). A few years passed before a chemically modified analog resistant to nucleases, methylphosphonate (PMe), was applied by Ts'o and co-workers (3). However, this analog also had problems since it was uncharged and relatively insoluble in water (4).

The first analog applied successfully as an antisense inhibitor that was both resistant to nucleases and water-soluble was the phosphorothioate (PS) analog (Figure 1) (4,5). This antisense oligonucleotide (ASO) was used against many biological systems and was the basis of several drug applications approved by the Food and Drug Administration (FDA) (5,6).

Over time new analogs were developed and tested (6), such as the peptide nucleic acid (PNA) (7), locked nucleic acid (LNA) (8), morpholino nucleic acid (PMO) (8) and 2′-OMe analog (6,9) (Figure 1). Naturally, each of the authors using these analogs touted their particular analog as superior to the

Received: October 24, 2023. **Revised:** September 5, 2024. **Editorial Decision:** October 16, 2024. **Accepted:** October 30, 2024

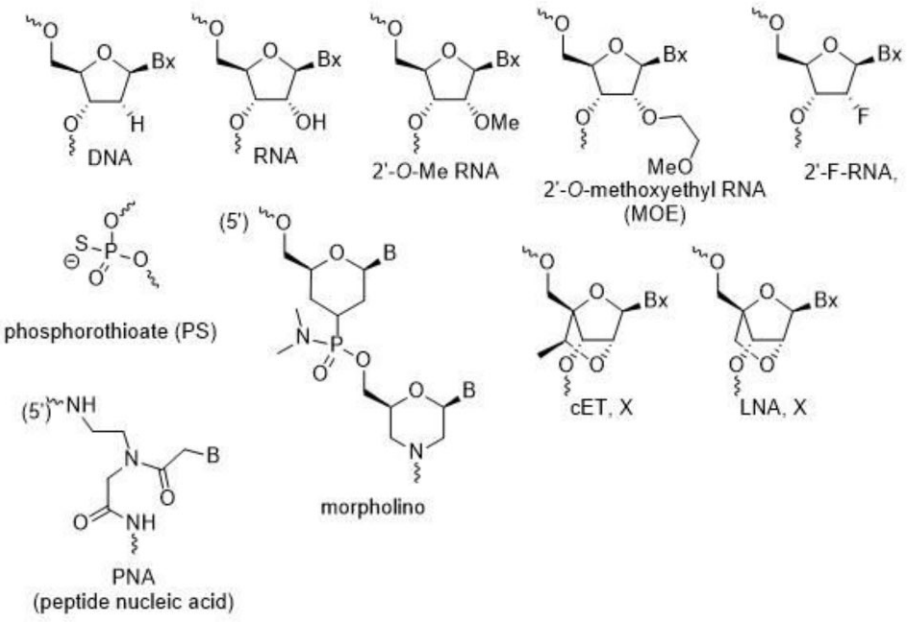

Figure 1. Structures of DNA (PO) and eight chemically modified analogs used in this study: phosphorothioate (PS), 2′-OMe, 2′-F, 2′-MOE, peptide nucleic acid (PNA), locked nucleic acid (LNA), constrained nucleic acid (cET) and morpholino (PMO) analogs.

others. However, objective comparative methodology has yet to be available to evaluate the potential of all these analogs as antisense compounds. What is needed is an independent and common approach that measures the basis of the antisense method, namely the ability to duplex with a target mRNA. Subsequently, second-generation analogs were developed and tested (6), such as the PNA (7), LNA (8), PMO (8) and 2′-OMe analog (6,9) (Figure 1).

In the present work, we perform molecular dynamics (MD) (10,11) simulations of eight modifications commonly observed in the design of ASOs. The modifications were placed in the 5′ strand of the Drew–Dickerson dodecamer (DDD) with the sequence d(CGCGAATTCGCG)$_2$. To test the stability of the modifications to form hybrid structures, the complementary strand was either DNA (XNA–DNA) or RNA (XNA–RNA).

Materials and methods

The starting structure used for all the simulations presented in this work are based on the high-resolution X-ray crystal of the DDD with sequence d(CGCGAATTCGCG) from Schofield and collaborators (PDB 4C64) (12). Each modified residue was constructed using Biovia Discovery Studio Visualizer v23 (13). Charges of the modified structures were calculated using Gaussian 16 (14) with the HF/6–31G* level of theory and basis set. Additional parameterization and charge fitting were performed using the pyRED webserver (15). The LEaP program was used to generate initial AMBER topology and coordinate files using the OL15 (16–18) force field for DNA and OL3 (19,20) for RNA. Parameters for the phosphorothioate backbone were obtained from the Orozco group (21). PNA backbone parameters were obtained from the Trylska group (21). The general AMBER force field (GAFF2) was employed as a source for missing parameters (22). Each modified XNA was modeled with the DDD sequence and solvated with the optimal 4-point rigid water model (23) using a 10 Å buffer between the solute and the edge of a truncated octahedral periodic box. NaCl ions were added to neutralize the charge, and excess ions were added to reach a 150 mM final concentration. Ions were described with the Joung–Cheatham parameters (24). Initial relaxation of the geometry, heating and initial equilibration was performed using a nine-step protocol utilizing the AmberMDprep program (25). All simulations were performed at 310K using a Langevin dynamics thermostat (collision frequency of 0.01/ps) (26), Monte Carlo barostat and periodic boundary conditions. The SHAKE algorithm was employed to perform bond length constraints for hydrogen bound to heavy atoms (27). The hydrogen mass repartition (28) scheme allowed for a time step of 4 fs. The GPU implementation of pmemd was employed for all simulations as found in AMBER20 and AMBER22 (29,30). Analysis was performed with the GitHub version of CPPTRAJ (v6.15.0) (31,32). All simulated XNA systems were calculated using three independent runs, each 5 μs total sampling time. Clustering analysis was performed using the hierarchical algorithm utilizing only the central residues and a 3.5 Å epsilon value (33). Helicoidal information was calculated using the `nastruct` command as implemented in CPPTRAJ. The stacking percentage was calculated using Hayatshahi's methodology (34,35). Binding energy analysis using the modified 5′ strand as ligand and the 3′ (DNA or RNA) strand as the receptor was calculated using the MM-GBSA protocol as implemented in the MMPBSA.py script (36). The analysis of the loss of duplex formation was performed running five independent copies of ∼300 ns, each starting with a different seed value at different temperatures ranging from 300K up to 500K in 10 degree intervals. The same minimization, heating and production protocol was used for each temperature window. The information from all five independent copies was used to perform a hydrogen bond analysis between the hybrid duplexes, and the average of detected Watson–Crick (WC) contacts was calculated. The criterion to consider a fully formed WC contact was implemented in the CPPTRAJ `nastruct` analysis command based on the descriptions set by Babcok and Olson (37,38).

Results

It is important to mention that simulation convergence for this particular size of nucleic acids is achieved on the ∼3–5 μs time scale (10,33), and statistical confidence and reproducibility are enhanced with independent replicas for each simulation (39).

All the modeled systems generated stable duplexes with DNA and RNA strands (Figure 2). Visual inspection of the representative structures from the cluster analysis suggests high mobility and alternate non-duplex formations, mainly in the terminal base pairs. Fraying effects at both ends of nucleic acids from MD simulations have been routinely observed, even as deep as the sixth position towards the central base pairs (40). Quantitatively, the root mean square structural deviation is shown in Table 1, using as a reference the most populated cluster structure from the simulations of the crystal structure. The cET and LNA modifications present the highest deviation for the XNA–DNA hybrids. Both systems have a constrained furanose moiety that fixes the sugar pucker in the 3′-endo position (41,42). When these two modifications are duplexed with an RNA strand, the structural deviation is within ∼2.5–2.9 Å of the reference structure, which is expected due to the constrained position of the sugar pucker, which favors the RNA structure. The system with the 2′-O-methyl modification presents a deviation of 4.5 Å when paired with DNA due mainly to fraying effects, which are reduced when paired with RNA. Overall, the modifications present less duplex formation to DNA than to RNA, which suggests that interactions caused by either a tether in the C2' position, a constrained furanose ring or lack of it, as with the PNA, favors the interaction for RNA.

When the modified strand has the 2′-O-methoxyethyl tethers, the fluctuation of the oligo chain is strongly enhanced by ∼5 Å (Figure 3). The presence of this modification inflicts a load on the entire residue that is increased by the reorientation of each nucleotide to complement the DNA strand; hence, when in the presence of the RNA strand, the structural stress is greatly reduced, as observed by the root mean square fluctuation analysis. The fluctuations for the rest of the systems are ∼2–3 Å within each other, with an increase in dynamics at both ends of the two strands, as previously observed (16,17,43). The fluctuations are reduced within the central base pairs for most systems, with slight increases for the PNA and morpholino simulations as they adjust the backbone conformation to stabilize the pairing with the complementary strand.

Another induced structural deviation caused by the modifications in the XNA strand is the overall helical bend of the DNA and RNA hybrids (Figure 3, bottom). As expected, due to the high fluctuations observed in the previous analysis, the system with the 2′-MOE shows the highest range of bend values for DNA and RNA. Structures closer to the unmodified DNA or RNA controls are the 2′-F and the PS, due to the fluor atom's small influence in the furanose ring or the sulfur atom in the backbone. Modifications with the constrained furanose (cET and LNA) show lower bend angles that are more consistent in accommodating RNA, whereas the PNA seems to prefer to adopt a structure that is more favorable to form hybrids with DNA. Interestingly, the morpholino variant shows the flexibility to adopt conformations that could accommodate hybridization with either DNA or RNA.

Binding energy calculation using the MM-GBSA methodology of the modified oligos is presented in Table 2. Using the unmodified DNA–RNA duplexes as a control, we can observe that the PNA modification enhances the stability of the formation of the duplex with DNA and RNA by 42.6 and 43.1 kcal/mol, respectively. Both the systems with the furanose modifications (cET and LNA) increase the stability of the hybrid by an average of ∼7 kcal/mol for DNA and ∼14 kcal/mol for RNA.

To further compare how the modifications influence the structure and dynamics of the DNA and RNA hybrids, the stacking percentage was calculated for each base step for the modified strand (Figure 4). The increment in fluctuations is propagated to the rest of the bases, affecting the stacking stability through the simulation. Fraying effects and the breaking and re-formation of WC pairing in the terminal base pairs are observed for all the studied systems. High fluctuations and mobility are introduced by bulky substituents, mainly in the backbone, as observed primarily for the 2′-MOE modification in all the base steps. It is interesting to observe a lack of stacking in the 3–4 base step in most of the 2–3 step. This is due to a fraying effect that opens the end of the chain up to the fourth base to form a temporary four-base single strand; this frayed temporary single strand conserves the stacking between steps 2 and 3. In a similar way, the 3′ end of the modified strand frays, forming a temporary single strand but conserving the stacking in the 10–11 step. The loose stacking within central base pairs is formed mainly in transient rotations of the backbone that flip the nucleobase towards the major groove. The control simulations as well as the 2′-F and PS systems show a similar trend. No discernible stacking difference is observed between the DNA or RNA hybrids which could be theorized to be sequence dependent. Presented in Figure 5 is the radial distribution function of Na^+ ions averaged over all electronegative sites for each modified ASO. At short distances, the accumulation of positive ions is higher due to the interaction of the negative backbone. There is no significant difference observed regarding the accumulation of the cations from the simulations, in part because the overall backbone structure is formed by sequential monomers linked by negatively charged phosphate groups.

To further study the stability of the modified ASOs to form duplexes, a series of simulations at different temperatures was performed (Figure 6). In both instances, the modified backbone with the constrained furanose variants shows a more stable duplex formation, which is quite noticeable for cET and LNA when in the presence of the RNA strand. The 2′-MOE modification shows unfolding (loss of duplexation) at ∼380K for both DNA and RNA system modifications, showing the lowest H-bond hybridization profile, which could be explained by the increased fluctuations induced by the 2′-O-methoxyethyl chain acting as a ballast of the furanose ring. We carried out a literature search for melting temperatures of oligo analog duplexes and were unable to obtain a sufficient number of comparative values. Also the T_m depends on parameters such as oligo length and solution conditions (44).

From the base pair and base step helicoidal analysis (Table 3), it is observed that the 2′-MOE modification unwinds the duplex in both DNA and RNA, also reducing the overall rise values as observed for double-stranded RNA simulations (42). Overall, the 2′-F and PS modifications are in line with the control values due to the small influence on structure and dynamics introduced by these modified residues.

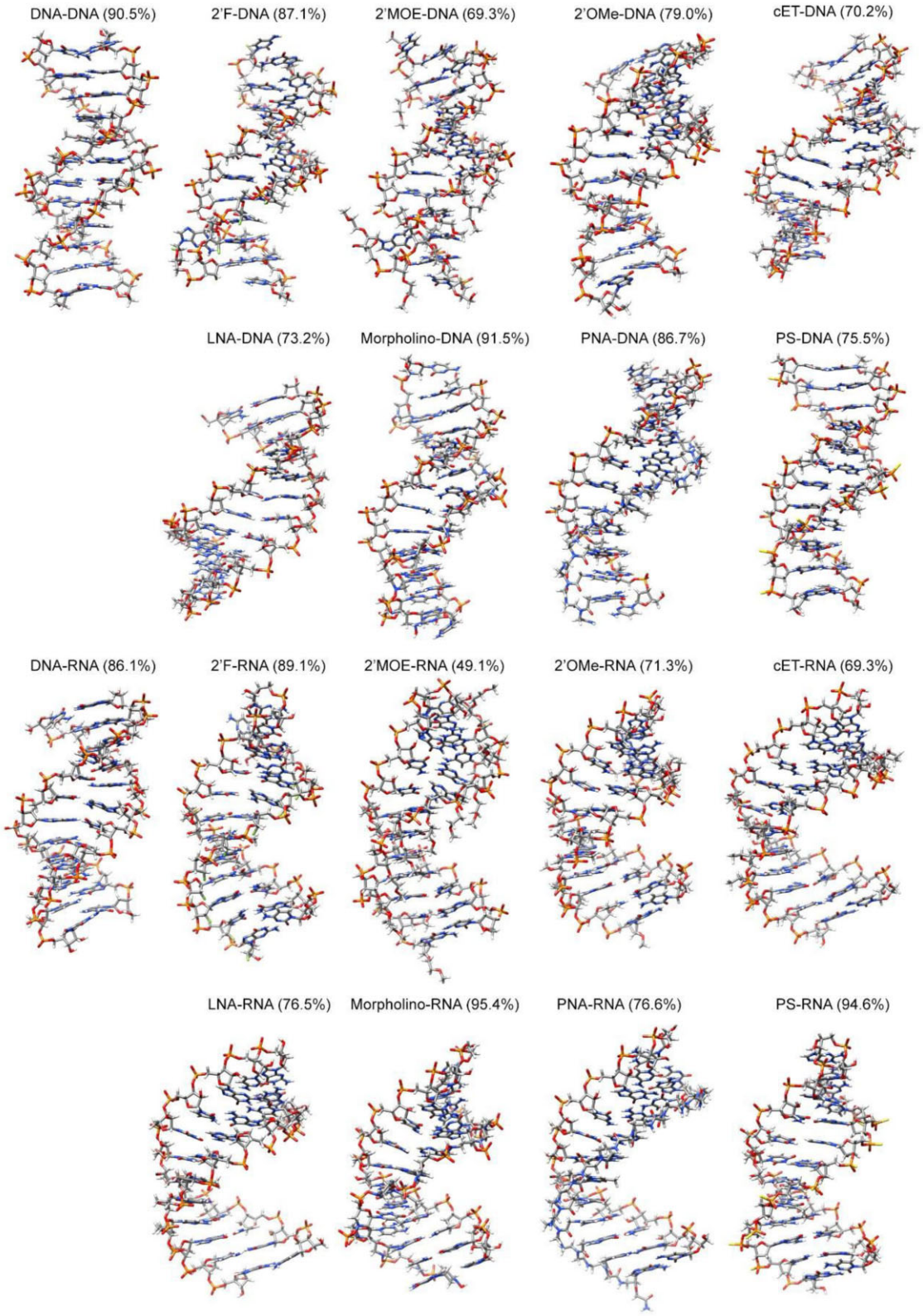

Figure 2. Depiction of the representative structure of the most populated cluster from the MD simulations. The fraction of the cluster out of the total frames calculated is reported in parentheses. Fraction percentage was calculated using all three replicas.

Table 1. Root mean square deviation values of the representative structure from the most populated cluster verus an average structure from MD simulations of the reference crystal structure

	XNA–DNA	XNA–RNA
C2′-F	1.7	2.1
C2′-MOE	1.9	2.6
C2′-OMe	4.5	1.4
cET	7.4	2.5
LNA	9.5	2.9
Morpholino	1.5	1.4
PNA	3.4	2.4
PS	1.4	2.1

The comparison was calculated using all the trajectory frames from the three independent copies. All atoms are included in the analysis.

The shear, stretch and stagger helicoidal parameters, normally associated with the alignment of base pairing, are close to the control values for all the modifications in DNA and RNA duplex cases.

For the constrained cET and LNA variants, which favor the pairing with RNA, the helicoidal values obtained from the DNA hybrid show more A-like values: reduction of the helical twist to a value of ∼25.0°, inclination of ∼12.5°, propeller of ∼7.0° and increased *x*-displacement of ∼5–6 Å.

In the previous analysis presented in this work, we have observed the ability of the morpholino variant to accommodate both DNA and RNA complementary strands. The helicoidal parameters for this modification show values close to the control, regardless of the complementary strand. For example, the propeller angle for the morpholino–DNA hybrid is –11.3, close to the control of –9.3, and for the RNA hybrid it is –12.5, close to the measured value of –10.5 for the control. Another example is observed with the grooves, where the major groove of the morpholino–DNA hybrid is 19.0, close to 19.3 for the control and 19.4 for the RNA hybrid, close to the control value of 19.2 Å. The main differences between the morpholino modification and the control values are observed in buckle, tip and roll.

The PNA hybrid forms a stable duplex with DNA and RNA. With a root mean square differentiation difference of 3.4 and 2.5 for DNA and RNA, respectively, the main difference consists of lower twist values, widening the major groove and forming a shallow minor groove. Overall, the helicoidal parameters produce a more A-like type of duplex, as reported in previous MD simulations (45,46).

The groove width is highly correlated with the capacity of nucleic acid structures to bind to proteins. Hence, the type of modification of the ASO, which modulates the groove width and depth to an extent, is important to consider.

The Zp value is a useful measure to study whether a particular base pair is in the anti-conformation (Zp > 0) or syn conformation (Zp < 0) (47). This also translates as a method to assign A- or B-form hybridization qualitatively (48). In Table 3, we present the average values over the 11 base steps for each modified ASO. The controls show a Zp value of –0.25 and 0.89 for DNA–DNA and DNA–RNA, respectively. When the modified ASOs are hybridized with DNA, the flexible modifications to remain in a B-like conformation are 2′-F, 2′-MOE, morpholino and PS, corresponding to the previous helical bend analysis. It is interesting to notice that the XNA–DNA system with 2′-OMe shows an A-type configuration (Zp = 0.98), suggesting that the presence of the O-methyl group mimics the 2′-hydroxyl group found in DNA, hence driving the conformation to more RNA like. The constrained systems cET and LNA, which favor the anti-conformation due to the covalent bridge in the furanose ring, show A-type conformations with Zp values of 1.5 each. This is highly augmented when both cET and LNA are hybridized with RNA, when the Zp values increase to 2.3 and 2.4, respectively. The system with the 2′-OMe also increases the A-type configuration, preferring to form a duplex with an RNA strand. The rest of the modified systems accommodate the hybridization with RNA, forming an A-form duplex.

Discussion

The mechanism of antisense action involves the binding of the ASO to its complementary target site in mRNA, thus blocking its expression. Another mechanism involving RNase H action has also been described, in which this enzyme cleaves the RNA strand in a DNA–RNA duplex (49,50). Presumably this endogenous mechanism results from the need for the cell to remove unwanted DNA–RNA duplexes. RNase H activity varies according to the cellular system and the DNA analog used to prevent nuclease degradation. However, since the RNase H activity also depends on the formation of the DNA–RNA duplex, the comparative MD calculations of duplexation of different oligomer analogs should still reflect their relative antisense efficacy.

The initial comparison of the PS analog with the natural PO of DNA in duplexation using MD calculations (51) has improved the MD methodology (10). Several MD studies of individual ASO analogs have been reported, including PNA (52,53), LNA (54), MOE (55) and 2′-OMe and LNA (56). Also, a study of different PS stereoisomers has been carried out using computational methods (21). However, these studies were self-contained and lacked comparison with other analogs also used as ASO analogs. We here report such a comparative MD study using eight of the analogs widely used for antisense inhibition applications with the natural phosphodiester as a control.

Although the ability to duplex with a target mRNA sequence is crucial for an antisense mechanism, other factors play a role in the efficacy of ASOs. Among these are the following. (i) Cell uptake; the ASO analog must be able to enter the cell. Such an ability varies from analog to analog and may also be partially dependent on charge and sequence. (ii) *In vivo* distribution can vary with the analog type and the organism. Nevertheless, the *sine qua non* for an antisense inhibition is the ability of the putative ASO drug to duplex effectively with its target sequence.

We mainly carried out this MD study because there is no comparative study published in which most oligo analogs used for antisense applications have been directly compared regarding their duplex formation with RNA and/or DNA under the same conditions. While this is a study *in silico*, it nevertheless provides a useful comparison. It is of interest to compare the results of this study with several experimental comparisons of duplex formation with antisense analogs.

Oligopeptides incorporating nucleic acid bases instead of typical amino acid side chains have been developed for antisense applications (7). These peptides offer resistance to nucleases, are water soluble and can be easily conjugated with cell-penetrating peptides to enhance cellular uptake (57,58).

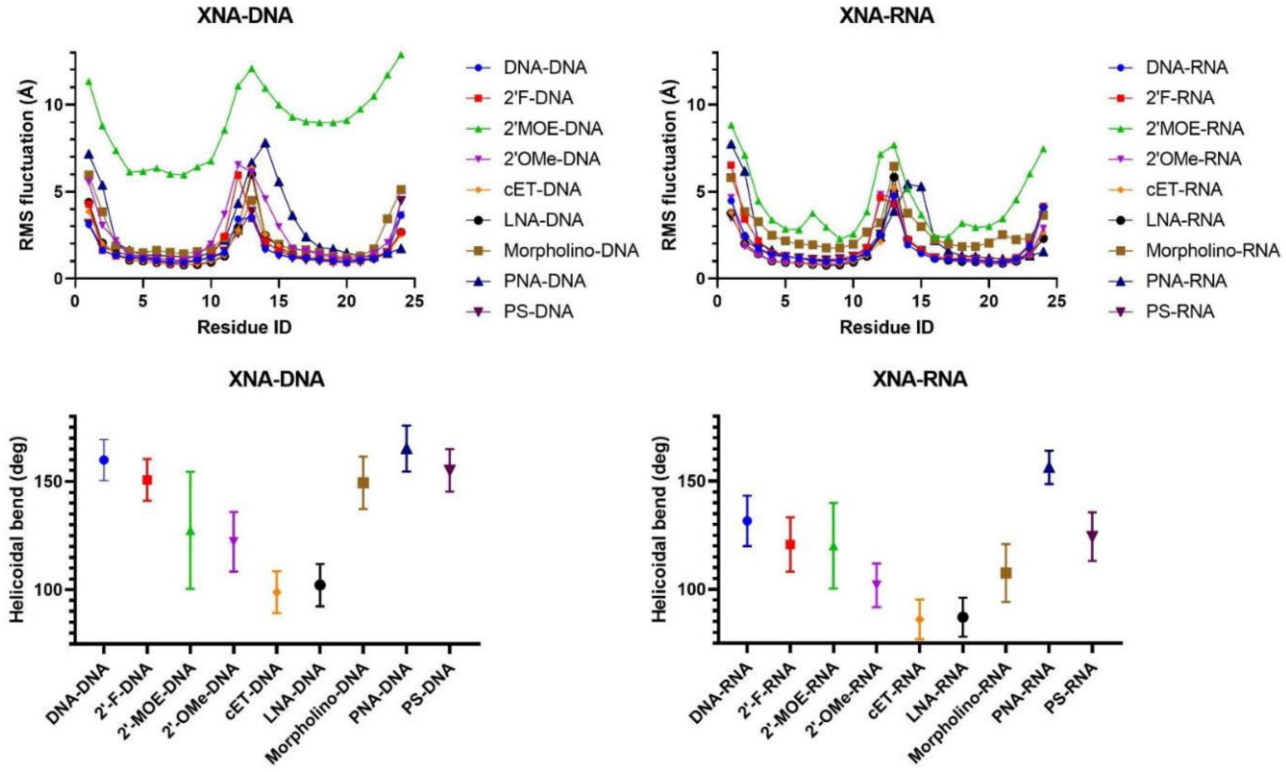

Figure 3. Top row: root mean square fluctuation analysis. Bottom row: helicoidal bend analysis as calculated using the terminal base and the central base pairs as anchors. Data were calculated using all the frames from the three independent simulations; error bars represent the SD.

Table 2. Binding energy values for the modified DNA and RNA hybrids

	DNA–DNA	DNA–RNA
Controls	– 103.3	– 105.1
	XNA–DNA	XNA–RNA
2′-F	– 95.3	– 96.9
2′-MOE	– 67.9	– 84.8
2′-OMe	– 93.8	– 103.4
cET	– 112.0	– 120.5
LNA	– 109.4	– 117.3
Morpholino	– 90.9	– 98.8
PNA	– 145.9	– 148.2
PS	– 107.6	– 104.0

Calculation was performed using every 10th frame from the three independent replicas.

They have been shown to be efficient at duplex formation with RNA (59,60). Antisense PNAs have successfully targeted various biological systems, including bacteria (61).

LNAs were engineered to be completely resistant to nucleases by locking the sugar moiety's structure (Figure 1), thereby reducing the flexibility of the ribo-furanoside ring and improving duplex stability (8). Comparisons by Kurreck *et al.* have shown LNAs to outperform PS oligos, although production cost and complexity are factors to consider (62). Other studies have also touted LNAs' superiority over other ASOs (63).

Morpholino analogs of oligonucleotides, designed to mimic natural structures (Figure 1), were developed by Summerton and colleagues. They claim superiority over other analogs in terms of antisense activity and RNase H function, particularly surpassing PS analogs (64–66). Comparative studies among PNA, LNA and morpholino analogs have highlighted distinct advantages for each (67,68), with morpholinos finding therapeutic application across diverse biological systems (69).

Early research was conducted with ribo-oligomers with-substitutions at the 2'-hydroxyl position (Figure 1), such as methyl or other alkyl groups, as potential ASOs. These modifications are known for their nuclease resistance and have become a major focus of research and development (70). For instance, 2′-OMe analogs have been used effectively to silence portions of the human β-globin gene (71).

Further advancements include the use of 2′-O-alkyl-RNA analogs in RNA biochemistry (72), as well as hybrid approaches combining 2′-O-alkyl ribo- and deoxy-polymers to enhance RNase H activity (73). Chimeric ASO analogs, combining PS oligos with 2′-O-alkyl co-polymers, have shown promise in various applications, including treating muscular dystrophy (74–76). Such combinations aim to improve mRNA degradation through enhanced RNase H activity (77).

Recent innovations include the introduction of 2′-fluoroadenosine in ribozymes (78), and the synthesis of uniformly modified 2′-deoxy-2′-fluoro PS oligos for highly specific RNA targeting (79). Recent discoveries have favored 2-MOE and 2′4′-constrained ethyl (cET) modifications, similar to LNAs, alongside GalNAC conjugates for ASOs (80). Their work has also led to the concept of gapmers, where 2′-O-alkyl PS analogs form the 'wings' and a PS oligo constitutes the 'gap', optimizing RNase H activity (81).

Overall, while numerous variations exist, the consensus supports the future of RNA oligo analogs. Notably, applications by Crooke and collaborators often target pre-mRNA and exon–intron junctions, addressing abnormal gene expression efficiently (82).

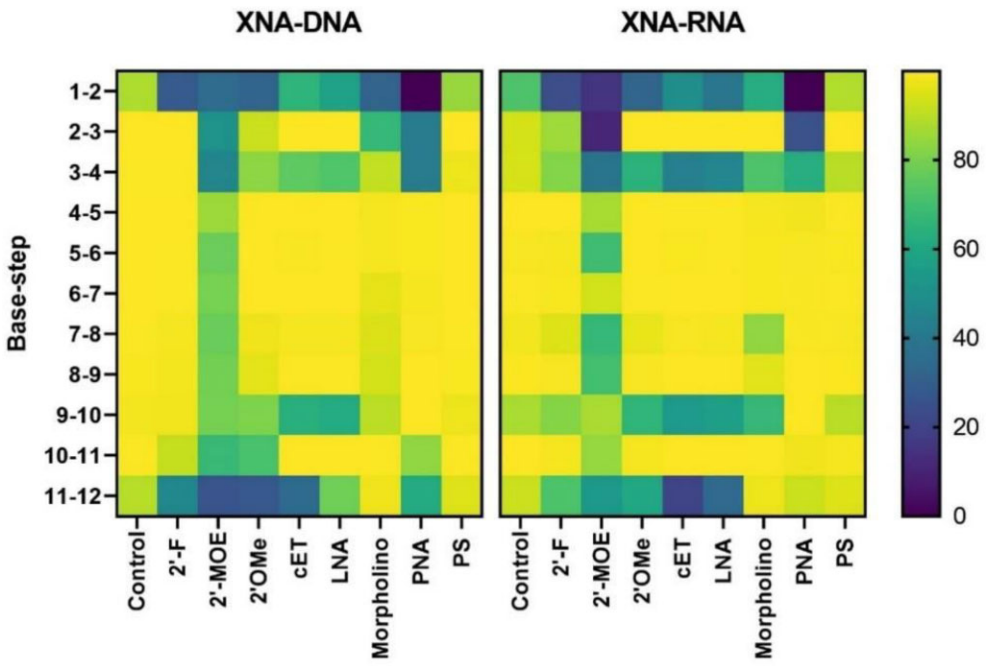

Figure 4. Per-step stacking percentages for the modified DNA and RNA duplexes. Analysis was performed using the full trajectory data from the three independent replicas.

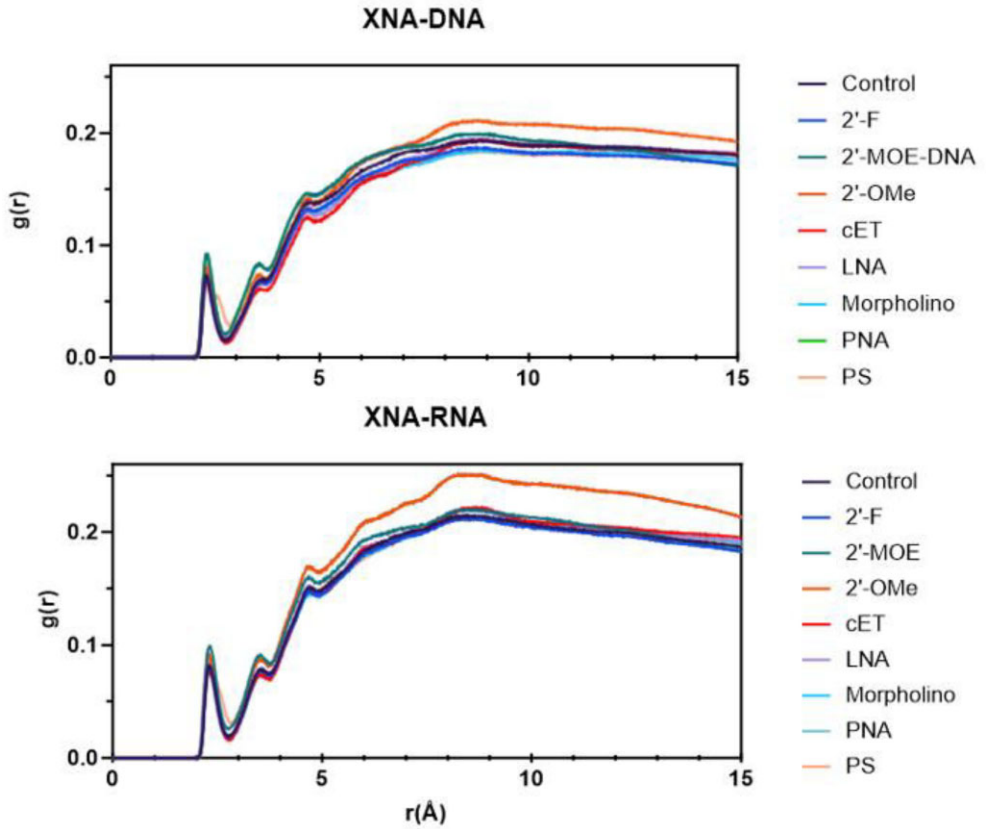

Figure 5. Radial distribution function of Na^+ ions. Analysis was performed using all the frames from the three independent replicas.

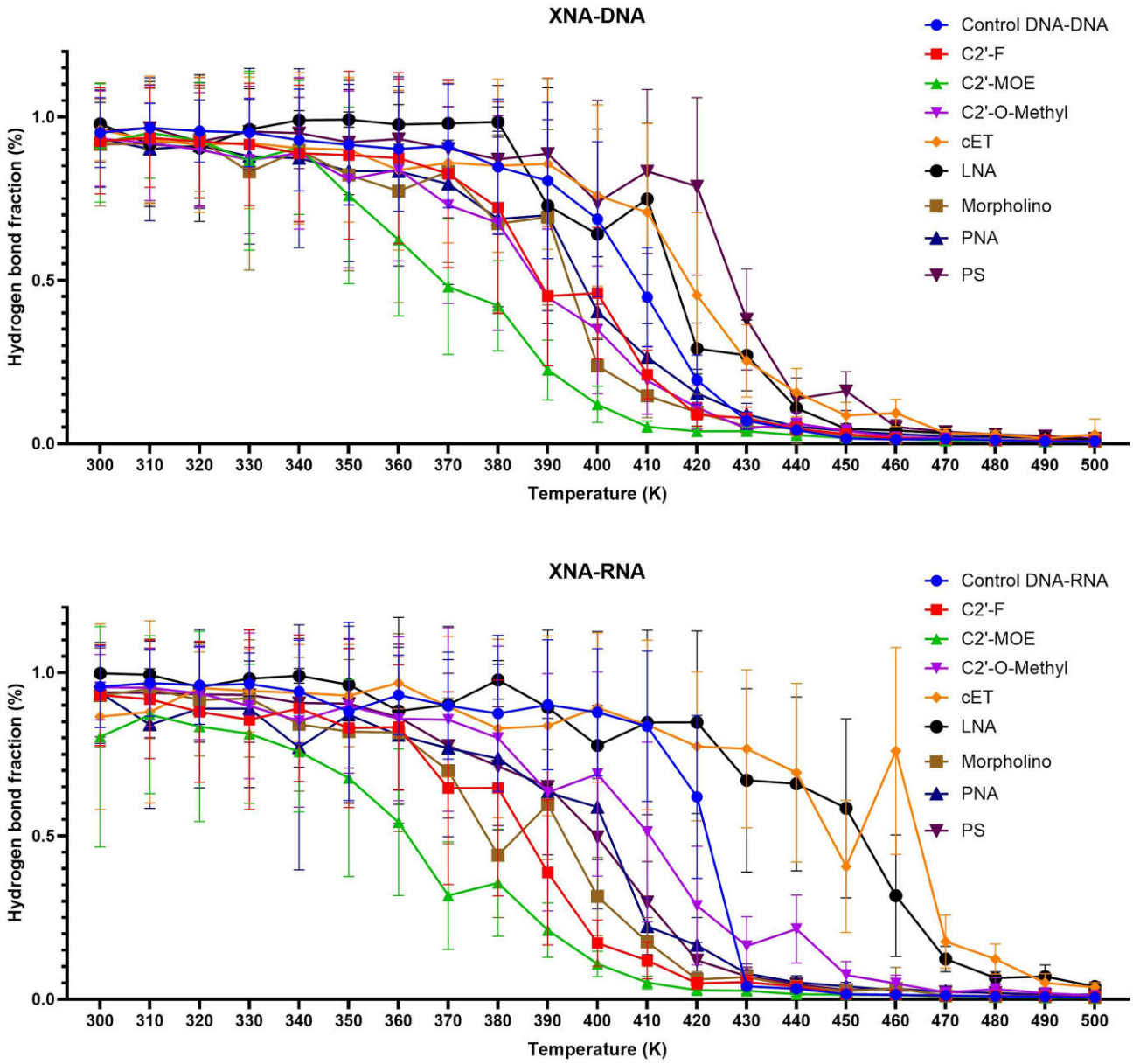

Figure 6. WC hydrogen-bond fraction counts for XNA–DNA (top) and XNA–RNA (bottom) at different temperatures. The double-stranded fraction corresponds to the number of WC-type hydrogen bonds between strands. Data points are average values from five independent simulations; bars show the standard deviation.

Conclusions

This work presents the results of multi-microsecond molecular dynamics simulations of a set of commonly used nucleic acid modifications for antisense therapy. The ability of the modifications to form stable duplexes with DNA and RNA was studied based upon structural changes, helicoidal analysis, binding energy and thermal stability. Overall, the furanose-constrained modifications cET and LNA present structural and thermal stability to accommodate DNA and RNA complementary strands. The small fingerprint of the modification (the 2′-O-methoxyethyl bridge in the furanose) decreases fluctuations, allowing for more stable base pairing. This is also observed with the PS, 2′-F and 2′-OMe for which, due to the small size of the modification, fluctuations are moderate and allow for stable duplex formation. On the other hand, the 2′-MOE introduces a high level of fluctuations due to the 2′-O-methoxyethyl chain. This reduces stability and enhances pairing dynamics, thus increasing the probability of fraying and breaking WC bonds. The PNA and morpholino cases were observed to adopt both DNA- and RNA-like conformations, which is due to the increased degrees of freedom, although this flexibility allows for the PNA to also increase in fluctuations that, in turn, enhance fraying and breaking of WC pairing. These effects are reduced considerably by the morpholino modification. In conclusion, from molecular dynamics simulations using recent methodologies and a set of force fields, and considering both structural deviations and binding affinity, the overall preference of hybrid strand formations is suggested as PNA > cET/LNA > PS/2′-F/2′-OMe > morpholino > 2′-MOE. It is important to mention that this study only focuses on the capabilities of the modifications to form complementary duplexes with DNA and RNA. A clear follow-up work

Table 3. Per-base and per-step helicoidal parameters for the control structures and the XNA–DNA (bottom) and XNA–RNA (top) modifications

	XNA–RNA									
	Shear (Å)	**Stretch (Å)**	**Stagger (Å)**	**Buckle (°)**	**Prop (°)**	**Opening (°)**	***x*-displacement (Å)**	***y*-displacement (Å)**	**Inclination (°)**	**Tip (°)**
Control	0.05	−0.04	−0.09	5.90	−10.58	0.25	−2.91	−0.15	11.90	3.89
2′-F	0.02	−0.01	−0.11	4.17	−9.60	0.39	−3.48	−0.09	13.47	2.77
2′-MOE	0.00	−0.02	−0.01	3.62	−2.15	0.94	−2.05	−0.37	8.78	3.74
2′-OMe	−0.06	−0.02	−0.09	−1.87	−9.63	−0.08	−4.79	−0.04	15.05	−0.98
cET	−0.12	0.12	−0.18	−6.27	−7.41	−0.93	−6.70	−0.87	15.15	−3.97
LNA	−0.06	−0.02	−0.05	−6.76	−7.54	0.43	−6.61	−0.87	13.61	−3.82
Morpholino	−0.04	−0.01	−0.01	−3.04	−12.57	0.67	−3.90	−0.09	13.81	−3.85
PNA	−0.03	−0.04	−0.08	−3.04	−7.40	−0.39	−5.01	−0.08	7.90	−4.09
PS	0.03	−0.02	−0.09	1.03	−11.59	0.40	−3.32	−0.20	13.32	3.92
	Shift (Å)	**Slide (Å)**	**Rise (Å)**	**Tilt (°)**	**Roll (°)**	**Twist (°)**	**Major groove (Å)**	**Minor groove (Å)**	**Zp (Å)**	
Control	−0.15	−0.96	3.28	−2.41	6.86	30.26	19.27	12.75	0.89	
2′-F	−0.13	−1.20	3.25	−1.58	7.29	29.29	19.01	12.58	1.06	
2′-MOE	−0.09	−0.59	2.25	−1.56	4.68	18.26	14.00	9.11	0.52	
2′-OMe	0.06	−1.84	3.32	0.54	8.22	29.60	18.94	13.34	2.25	
cET	0.60	−2.38	3.29	1.90	7.08	25.23	18.01	12.33	2.35	
LNA	0.60	−2.40	3.30	1.92	7.90	25.32	19.70	13.37	2.40	
Morpholino	0.15	−1.48	3.14	1.53	8.29	29.27	19.49	12.75	0.76	
PNA	0.69	−2.02	3.23	0.94	6.47	23.86	n/a	13.15	n/a	
PS	−0.12	−1.16	3.30	−2.14	7.40	30.47	19.49	12.89	0.93	
	XNA–DNA									
	Shear (Å)	**Stretch (Å)**	**Stagger (Å)**	**Buckle (°)**	**Prop. (°)**	**Opening (°)**	***x*-displacement (Å)**	***y*-displacement (Å)**	**Inclination (°)**	**Tip (°)**
Control	0.00	−0.03	0.01	0.29	−9.01	−0.03	−0.63	0.01	3.75	−0.09
2′-F	−0.04	−0.02	−0.01	−0.80	−10.18	−0.09	−1.06	−0.02	5.79	−0.58
2′-MOE	−0.05	0.00	0.02	−1.77	−6.77	0.34	−0.85	0.00	3.40	0.13
2′-OMe	−0.09	−0.05	−0.05	−7.20	−8.58	0.10	−3.16	0.02	11.92	−3.67
cET	−0.11	−0.01	−0.05	−11.85	−7.10	0.25	−6.05	−0.53	12.54	−6.69
LNA	−0.14	0.09	−0.17	−11.46	−6.88	−1.04	−5.92	−0.46	12.41	−7.01
Morpholino	−0.09	0.00	0.06	−7.17	−11.31	−1.31	−1.83	0.21	6.33	−7.18
PNA	−0.05	−0.06	0.01	−9.68	−9.71	0.51	−3.01	0.01	−11.30	−0.65
PS	−0.02	−0.03	0.08	−1.06	−9.64	−0.31	−1.23	−0.04	3.37	−0.56
	Shift (Å)	**Slide (Å)**	**Rise (Å)**	**Tilt (°)**	**Roll (°)**	**Twist (°)**	**Major groove (Å)**	**Minor groove (Å)**	**Zp (Å)**	
Control	0.00	−0.12	3.29	0.06	2.00	34.22	19.36	12.22	−0.25	
2′-F	0.04	−0.24	3.26	0.28	2.96	32.69	19.28	12.00	−0.37	
2′-MOE	−0.01	−0.22	2.29	−0.16	1.59	22.02	13.57	8.41	−0.25	
2′-OMe	0.19	−1.08	3.02	2.04	6.53	27.51	17.72	11.70	0.98	
cET	0.61	−2.12	3.31	3.11	5.80	24.99	20.36	13.03	1.50	
LNA	0.60	−2.11	3.32	3.34	5.82	25.41	18.79	12.11	1.51	
Morpholino	0.08	−0.60	3.08	2.48	4.64	30.77	19.07	11.95	−0.43	
PNA	0.79	−1.05	3.36	2.30	4.33	27.22	n/a	13.16	n/a	
PS	0.05	−0.50	3.31	0.35	1.88	33.42	19.74	12.45	−0.09	

Minor groove width for the PNA modification is measured as the distance between the phosphate atom of the antisense strand and the glycine carbon of the pseudopeptide backbone.

will be the study of the modifications presented in this work with regard to how they affect protein binding with nucleases, for example RNase H1, argonaute 2 and the Dicer system, using computational tools and MD simulations. This will aid in the design of novel modifications for ASO therapeutics.

Data availability

All datasets and codes for analysis used in the manuscript and analysis are available upon request from the authors.

Acknowledgements

We thank the Center for High-Performance Computing at the University of Utah for computing resources.

Funding

No external funding.

Conflict of interest statement

The authors declare that there is no conflict of interest.

References

1. Zamecnik,P.C. and Stephenson,M.L. (1978) Inhibition of Rous sarcoma virus replication and cell transformation by a specific oligodeoxynucleotide. *Proc. Natl Acad. Sci. USA*, **75**, 280–284.
2. Ott,C. and Eckstein,F. (1987) Protection of oligonucleotide primers agaisnt degradation by DNA polymerase. *Biochemistry*, **26**, 8237–8241.

3. Jayaraman,K., McParland,K., Miller,P. and Ts'o,P.O.P. (1981) Selective inhibition of *Escherichia coli* protein synthesis and growth by nonionic oligonucleotides complementary to the 3′ end of 16S rRNA. *Proc. Natl Acad. Sci. USA*, **78**, 1537–1541.
4. Matsukura,M., Zon,G., Shinozuka,K., Roberts-Guroff,M., Stein,C.A., Mitsuya,H., Wong-Staal,F., Cohen,J.S. and Broder,S.A. (1989) Regulation of viral expression of HIV in vitro by antisense phosphorothioate oligodeoxynucleotide against rev (art/trs) in chronically infected cells. *Proc. Natl Acad. Sci. USA*, **86**, 4244–4248.
5. Stein,C.A. and Castanotto,D. (2017) FDA-approved oligonucleotide therapies in 2017. *Mol. Ther.*, **25**, 1069–1075.
6. Cohen,J.S. (2021) History of research on antisense oligonucleotide analogs. *Substantia (Intl J. Hist. Chem.)*, **5**, 9–25.
7. Egholm,M., Buchardt,O., Nielsen,P.E. and Berg,R.H. (1992) Peptide nucleic acids (PNA). Oligonucleotide analogs with an achiral peptide backbone. *J. Am. Chem. Soc.*, **224**, 1895–1897.
8. Wengel,J., Koshkin,A., Singh,S.K., Nielsen,P., Meldgaard,M., Rajwanshi,V.K., Kumar,R., Skouv,J., Nielsen,C.B. and Jacobsen,J.P. (1999) LNA (locked nucleic acid). *Nucleosides Nucleotides Nucleic Acids* , **18**, 1365–1370.
9. Wagner,E., Oberhauser,B., Holzner,A., Brunar,H., Issakides,G., Schaffner,G., Cotten,M., Knollmüller,M. and Noe,C.R. (1991) A simple procedure for the preparation of protected 2'-O-methyl or 2'-O-ethyl ribonucleoside-3'-O-phosphoramidites. *Nucleic Acids Res.*, **19**, 5965–5971.
10. Galindo-Murillo,R., Roe,D.R. and Cheatham,T.E. 3rd (2015) Convergence and reproducibility in molecular dynamics simulations of the DNA duplex d(GCACGAACGAACGAACGC). *Biochim. Biophys. Acta*, **1850**, 1041–1058.
11. Galindo-Murillo,R., Cohen,J.S. and Akabayov,B. (2020) Molecular dynamics simulations of duplexation of acyclic analogs of nucleic acids for antisense inhibition. *Mol. Ther. Nucleic Acids*, **23**, 527–535.
12. Lercher,L., McDonough,M.A., El-Sagheer,A.H., Thalhammer,A., Kriaucionis,S., Brown,T. and Schofield,C.J. (2014) Structural insights into how 5-hydroxymethylation influences transcription factor binding. *Chem. Commun.*, **50**, 1794–1796.
13. Accelrys Software Inc. Discovery Studio Visualizer. Accelrys Software Inc. (2009)
14. Frisch,M.J., Trucks,G.W., Schlegel,H.B., Scuseria,G.E., Robb,M.A., Cheeseman,J.R., Scalmani,G., Barone,V., Petersson,G.A., Nakatsuji,X., *et al.* (2009) In: *Gaussian 09, Revision D.01*. Gaussian, Inc.: Wallingford, CT.
15. Vanquelef,E., Simon,S., Marquant,G., Garcia,E., Klimerak,G., Delepine,J.C., Cieplak,P. and Dupradeau,F.-Y. (2011) R.E.D. Server: a web service for deriving RESP and ESP charges and building force field libraries for new molecules and molecular fragments. *Nucleic Acids Res.*, **39**, W511–W517.
16. Dans,P.D., Ivani,I., Hospital,A., Portella,G., González,C. and Orozco,M. (2017) How accurate are accurate force-fields for B-DNA?*Nucleic Acids Res.*, **45**, gkw1355.
17. Galindo-Murillo,R., Robertson,J.C., Zgarbová,M., Šponer,J., Jurečka,P. and Cheatham,T.E. 3rd (2016) Assessing the current state of Amber force field modifications for DNA. *J. Chem. Theory Comput.*, **12**, 4114–4127.
18. Zgarbová,M., Šponer,J., Otyepka,M., Cheatham,T.E. 3rd, Galindo-Murillo,R. and Jurečka,P. (2015) Refinement of the sugar-phosphate backbone torsion beta for AMBER force fields improves the description of Z- and B-DNA. *J. Chem. Theory Comput.*, **11**, 5723–5736.
19. Sponer,J., Bussi,G., Krepl,M., Banas,P., Bottaro,S., Cunha,R.A., Gil-Ley,A., Pinamonti,G., Poblete,S., Jurečka,P., *et al.* (2018) RNA structural dynamics as captured by molecular simulations: a comprehensive overview. *Chem. Rev*, **118**, 4177–4338.
20. Šponer,J., Banáš,P., Jurečka,P., Zgarbová,M., Kührová,P., Havrila,M., Krepl,M., Stadlbauer,P. and Otyepka,M. (2014) Molecular dynamics simulations of nucleic acids. From tetranucleotides to the ribosome. *J. Phys. Chem. Lett.*, **5**, 1771–1782.
21. Genna,V., Iglesias-Fernandez,J., Reyes-Fraile,L., Villegas,N., Guckian,K., Seth,P., Wan,B., Cabrero,C., Terrazas,M., Brun-Heath,I., *et al.* (2023) Controlled sulfur-based engineering confers mouldability to phosphorothioate antisense oligonucleotides. *Nucleic Acids Res.*, **51**, 4713–4725.
22. Wang,J., Wolf,R.M., Caldwell,J.W., Kollman,P.A. and Case,D.A. (2004) Development and testing of a general Amber force field. *J. Comput. Chem.*, **25**, 1157–1174.
23. Izadi,S., Anandakrishnan,R. and Onufriev,A.V. (2014) Building water models: a different approach. *J. Phys. Chem. Lett.*, **5**, 3863–3871.
24. Joung,I.S. and Cheatham,T.E. 3rd (2008) Determination of alkali and halide monovalent ion parameters for use in explicitly solvated biomolecular simulations. *J. Phys. Chem. B*, **112**, 9020–9041.
25. Roe,D.R. and Brooks,B.R. (2020) A protocol for preparing explicitly solvated systems for stable molecular dynamics simulations. *J. Chem. Phys.*, **153**, 054123.
26. Pastor,R.W., Brooks,B.R. and Szabo,A. (1988) An analysis of the accuracy of Langevin and molecular dynamics algorithms. *Mol. Phys.*, **65**, 1409–1419.
27. Ryckaert,J.-P., Ciccotti,G. and Berendsen,H.J.C. (1977) Numerical integration of the Cartesian equations of motion of a system with constraints: molecular dynamics of n-alkanes. *J. Comput. Phys.*, **23**, 327–341.
28. Hopkins,C.W., Le Grand,S., Walker,R.C. and Roitberg,A.E. (2015) Long time step molecular dynamics through hydrogen mass repartitioning. *J. Chem. Theory Comput.*, **11**, 1864–1874.
29. Götz,A.W., Williamson,M.J., Xu,D., Poole,D., Le Grand,S. and Walker,R.C. (2012) Routine microsecond molecular dynamics simulations with AMBER on GPUs. 1. Generalized born. *J. Chem. Theory Comput.*, **8**, 1542–1555.
30. Salomon-Ferrer,R., Götz,A.W., Poole,D., Le Grand,S. and Walker,R.C. (2013) Routine microsecond molecular dynamics simulations with AMBER on GPUs. 2. Explicit solvent particle mesh Ewald. *J. Chem. Theory Comput.*, **9**, 3878–3888.
31. Roe,D.R. and Cheatham,T.E. 3rd (2013) PTRAJ and CPPTRAJ: software for processing and analysis of molecular dynamics trajectory data. *J. Chem. Theory Comput.*, **9**, 3084–3095.
32. Roe,D.R. and Cheatham,T.E. 3rd (2018) Parallelization of CPPTRAJ enables large scale analysis of molecular dynamics trajectory data. *J. Comput. Chem.*, **39**, 2110–2117.
33. Galindo-Murillo,R., Roe,D.R. and Cheatham,T.E. 3rd (2014) On the absence of intra-helical DNA dynamics on the μs to ms timescale. *Nat. Commun.*, **5**, 5152.
34. Hayatshahi,H.S., Niel,M. and Henriksen,T.E.C. 3rd (2018) Consensus conformations of dinucleoside monophosphates described with well-converged molecular dynamics simulations. *J. Chem. Theory Comput.*, **14**, 1456–1470.
35. Kollman,P.A., Massova,I., Reyes,C.M., Kuhn,B., Huo,S., Chong,L., Lee,M., Lee,T., Duan,Y., Wang,W., *et al.* (2000) Calculating structures and free energies of complex molecules: combining molecular mechanics and continuum models. *Acc. Chem. Res.*, **33**, 889–897.
36. Miller,B.R., McGee,T.D., Swails,J.M., Homeyer,N., Gohlke,H. and Roitberg,A.E. (2012) MMPBSA.Py : an efficient program for end-state free energy calculations. *J. Chem. Theory Comput.*, **8**, 3314–3321.
37. Babcock,M.S., Pednault,E.P. and Olson,W.K. (1994) Nucleic acid structure analysis. Mathematics for local Cartesian and helical structure parameters that are truly comparable between structures. *J. Mol. Biol.*, **237**, 125–156.
38. Olson,W.K., Bansal,M., Burley,S.K., Dickerson,R.E., Gerstein,M., Harvey,S.C., Heinemann,U., Lu,X.J., Neidle,S., Shakked,Z., *et al.* (2001) A standard reference frame for the description of nucleic acid base-pair geometry. *J. Mol. Biol.*, **313**, 229–237.

39. Knapp,B., Ospina,L. and Deane,C.M. (2018) Avoiding false positive conclusions in molecular simulation: the importance of replicas. *J. Chem. Theory Comput.*, **14**, 6127–6138.
40. Galindo-Murillo,R. and Cheatham,T.E. 3rd. (2022) Transient Hoogsteen base pairs observed in unbiased molecular dynamics simulations of DNA. *J. Phys. Chem. Lett.*, **13**, 6283–6287.
41. Brad Wan,W. and Seth,P.P. (2016) The medicinal chemistry of therapeutic oligonucleotides. *J. Med. Chem.*, **59**, 9645–9667.
42. Liebl,K., Drsata,T., Lankas,F., Lipfert,J. and Zacharias,M. (2013) Explaining the striking difference in twist–stretch coupling between DNA and RNA: a comparative molecular dynamics analysis. *J. Chem. Phys.*, **139**, 155102.
43. Love,O., Galindo-Murillo,R., Zgarbová,M., Šponer,J., Jurečka,P. and Cheatham,T.E. (2023) Assessing the current state of Amber force field modifications for DNA. *J. Chem. Theory Comput.*, **19**, 4299–4307.
44. Stein,C.A., Subasinghe,C., Shinozuka,K. and Cohen,J.S. (1988) Physicochemical properties of phosphorothioate oligodeoxynucleotides. *Nucleic Acids Res.*, **16**, 3209–3221.
45. Autiero,I., Saviano,M. and Langella,E. (2014) Molecular dynamics simulations of PNA–PNA and PNA–DNA duplexes by the use of new parameters implemented in the GROMACS package: a conformational and dynamics study. *Phys. Chem. Chem. Phys.*, **16**, 1868–1874.
46. Nielsen,P.E. (2004) PNA technology. *Mol. Biotechnol.*, **26**, 233–248.
47. Tian,C., Kasavajhala,K., Belfon,K., Raguette,L., Huang,H., Migues,A.N., Bickel,J., Wang,Y., Pincay,J., Wu,Q., *et al.* (2019) Amino-acid-specific protein backbone parameters trained against quantum mechanics energy surfaces in solution. *J. Chem. Theory Comput.*, **16**, 528–552.
48. Kulkami,M. and Mukherjee,A. (2013) Sequence dependent free energy profiles of localized B- to A-form transition of DNA in water. *J. Chem. Phys.*, **139**, 155102.
49. Dagle,J.M., Walder,J.A. and Weeks,D.L. (1990) Targeted degradation of mRNA in Xenopus oocytes and embryos directed by modified oligonucleotides: studies of An2 and cyclin in embryogenesis. *Nucleic Acids Res.*, **18**, 4751–4757.
50. Walder,R.Y. and Walder,J.A. (1988) Role of RNase H in hybrid-arrested translation by antisense oligonucleotides. *Proc. Natl Acad. Sci. USA*, **85**, 5011–5015.
51. Jaroszewski,J.W., Syi,J.-L., Maizel,J. and Cohen,J.S. (1992) Towards rational design of antisense DNA: molecular modeling of phosphorothioate DNA analogues. *Anticancer Drug Design*, **7**, 253–262.
52. Soliva,R., Sherer,E., Luque,F.J., Laughton,C.A. and Orozco,M. (2000) Molecular dynamics simulations of PNA·DNA and PNA·RNA duplexes in aqueous solution. *J. Am. Chem. Soc.*, **122**, 5997–6008.
53. Verona,M.D., Verdolino,V., Palazzesi,F. and Corradini,R. (2017) Focus on PNA flexibility and RNA binding using molecular dynamics and metadynamics. *Sci. Rep.*, **7**, 42799.
54. Pande,V. and Nilsson,L. (2008) Insights into structure, dynamics and hydration of locked nucleic acid (LNA) strand-based duplexes from molecular dynamics simulations. *Nucleic Acids Res.*, **36**, 1508–1516.
55. Golyshev,V.M., Abramova,T.V., Pyshnyi,D.V. and Lomzov,A.A. (2019) Structure and hybridization properties of glycine morpholine oligomers in complexes with DNA and RNA: experimental and molecular dynamics studies. *J. Phys. Chem. B*, **123**, 10571–10581.
56. Yildirim,I., Kierzek,E., Kierzek,R. and Schatz,G.C. (2014) Interplay of LNA and 2'-O-methyl RNA in the structure and thermodynamics of RNA hybrid systems: a molecular dynamics study using the revised AMBER force field and comparison with experimental results. *J. Phys. Chem. B*, **118**, 14177–14187.
57. Mondhe,M., Chessher,A., Goh,S., Good,L. and Stach,J.E.M. (2014) Species-selective killing of bacteria by antimicrobial peptide–PNAs. *PLoS One*, **9**, e89082.
58. Patenge,N., Pappesch,R., Krawack,F., Walda,C., Abu Mraheil,M., Jacob,A., Hain,T. and Kreikemeyer,B. (2013) Inhibition of growth and gene expression by PNA–peptide conjugates in *Streptococcus pyogenes*. *Mol. Ther. Nucleic Acids*, **2**, e132.
59. Natsume,T., Ishikawa,Y., Dedachi,K., Tsukamoto,T. and Kurita,N.. (2007) Hybridization energies of double strands composed of DNA, RNA, PNA and LNA. *Chem. Phys. Lett.*, **434**, 133–138.
60. Crinelli,R.B.M., Gentilini,L., Palma,L. and Magnani,M. (2004) Locked nucleic acids (LNA): versatile tools for designing oligonucleotide decoys with high stability and affinity. *Curr. Drug Targets*, **5**, 745–752.
61. Nekhotiaeva,N., Awasthi,S.K., Nielsen,P.E. and Good,L. (2004) Inhibition of *Staphylococcus aureus* gene expression and growth using antisense peptide nucleic acids. *Mol. Ther.*, **10**, 652–659
62. Kurreck,J., Wyszko,E., Gillen,C. and Erdmann,V.A. (2002) Design of antisense oligonucleotides stabilized by locked nucleic acids. *Nucleic Acids Res.*, **30**, 1911–1918.
63. Wahlestedt,C., Salmi,P., Good,L., Kela,J., Johnsson,T., Hokfelt,T., Broberger,C., Porreca,F., Lai,J. and Ren,K. (2000) Potent and nontoxic antisense oligonucleotides containing locked nucleic acids. *Proc. Natl Acad. Sci. USA*, **97**, 5633–5638.
64. Summerton,J. and Weller,D. (1997) Morpholino antisense oligomers: design, preparation, and properties. *Antisense Nucleic Acid Drug Dev.*, **7**, 187–195.
65. Summerton,J., Stein,D., Huang,S.B., Matthews,P., Weller,S. and Partridge,M. (1997) Morpholino and phosphorothioate antisense oligomers compared in cell-free and in-cell systems. *Antisense Nucleic Acid Drug Dev.*, **7**, 63–70
66. Summerton,J. (1999) Morpholino antisense oligomers: the case for an RNase H-independent structural type. *Biochim. Biophys. Acta*, **1489**, 141–158.
67. Karkare,S. and Bhatnagar,D. (2006) Promising nucleic acid analogs and mimics: characteristic features and applications of PNA, LNA, and morpholino. *Appl. Microbiol. Biotechnol.*, **71**, 575–586
68. Qiao,W.C.,,Hao-Chun, Xie,H. and Levicky,R.. (2015) Surface vs. solution hybridization: effects of salt, temperature, and probe type. *Chem. Commun.*, **51**, 17245–17248.
69. Neuman,B.W., Stein,D.A., Kroeker,A.D., Churchill,M.J., Kim,A.M., Kuhn,P., Dawson,P., Moulton,H.M., Bestwick,R.K. and Iversen,P.L. (2005) Inhibition, escape, and attenuated growth of severe acute respiratory syndrome coronavirus treated with antisense morpholino oligomers. *J. Virol.*, **79**, 9665–9676
70. Iribarren,A.M., Sproat,B.S., Neuner,P., Sulston,I., Ryder,U. and Lamond,A.I. (1990) 2'-O-alkyl oligoribonucleotides as antisense probes. *Proc. Natl Acad. Sci. USA*, **87**, 7747–7751.
71. Mayeda,A., Hayase,Y., Inoue,H., Ohtsuka,E. and Ohshima,Y. (1990) Surveying cis-acting sequences of pre-mRNA by adding antisense 2′-O-methyl oligoribonucleotides to a splicing reaction. *J. Biochem.*, **108**, 399–405.
72. Lamond,A.I. and Sproat,B.S. (1993) Antisense oligonucleotides made of 2'-O-alkylRNA: their properties and applications in RNA biochemistry. *FEBS Lett.*, **325**, 123–127.
73. Monia,B.P., Lesnik,E.A., Gonzalez,C., Lima,W.F., McGee,D., Guinosso,C.J.,, Kawasaki,A.M., Cook,P.D. and Freier,S.M. (1993) Evaluation of 2'-modified oligonucleotides containing 2'-deoxy gaps as antisense inhibitors of gene expression. *J. Biol. Chem.*, **268**, 14514–14522.
74. Metelev,V., Lisziewicz,J. and Agrawal,S. (1994) Study of antisense oligonucleotide phosphorothioates containing segments of oligodeoxynucleotides and 2'-O-methyloligoribonucleotides. *Bioorg. Med. Chem. Lett.*, **4**, 2929–2934.
75. Yoo,B.H., Bochkareva,E., Bochkarev,A., Mou,T.-C. and Gray,D.M. (2004) 2'-O-methyl-modified phosphorothioate antisense oligonucleotides have reduced non-specific effects in vitro. *Nucleic Acids Res.*, **32**, 2008–2016
76. Aartsma-Rus,A. (2017) FDA approval of Nusinersen for spinal muscular atrophy makes 2016 the year of splice modulating oligonucleotides. *Nucleic Acid Ther.*, **27**, 67–69.

77. Giles,R.V. and Tidd,D.M. (1992) Enhanced RNase H activity with methylphosphonodiester/phosphodiester chimeric antisense oligodeoxynucleotides. *Anti Cancer Drug Des.*, **7**, 37–48.
78. Olsen,D.B., Benseler,F., Aurup,H., Pieken,W.A. and Eckstein,F. (1991) Study of a hammerhead ribozyme containing 2'-modified adenosine residues. *Biochemistry*, **30**, 9735–9741.
79. Kawasaki,A.M., Casper,M.D., Freier,S.M., Lesnik,E.A., Zounes,M.C., Cummins,L.L., Gonzalez,C. and Cook,P.D. (1993) Uniformly modified 2'-deoxy-2'-fluoro phosphorothioate oligonucleotides as nuclease-resistant antisense compounds with high affinity and specificity for RNA targets. *J. Med. Chem.*, **36**, 831–841.
80. MacLeod,A.R. and Crooke,S.T. (2017) RNA therapeutics in oncology: advances, challenges, and future directions. *J. Clin. Pharmacol.*, **57**, S43–S59.
81. Altmann,K.-H., Fabbrot,D., Dean,N.M., Geigert,T., Mania,P., Mullert,M. and Nickling,P. (1996) Second-generation antisense oligonucleotides: structure–activity relationships and the design of improved signal-transduction inhibitors. *Biochem. Soc. Trans.*, **24**, 630–637.
82. Bennett,C.F., Crooke,S.T., Manoharan,M., Wyatt,J.R., Baker,B.F., Monia,B.P., Freier,S.F., Mckay,R. and Karras,J.G. (2002) Alteration of cellular behavior by antisense modulation of mRNA processing. United States Patent, US20020049173.

Received: October 24, 2023. **Revised:** September 5, 2024. **Editorial Decision:** October 16, 2024. **Accepted:** October 30, 2024